

Multiscale interfacial mechanics of soft solids

Nicolas Bain,^{1,2,*} Lawrence A. Wilen,³ Dominic Gerber,² Mengjie Zu,⁴ Carl P. Goodrich,⁴ Senthilkumar Duraivel,⁵ Kaarthik Varma,⁵ Harsha Koganti,⁵ Robert W. Style,² and Eric R. Dufresne^{5,2}

¹Universite Claude Bernard Lyon 1, CNRS, Institut Lumière Matière, UMR5306, F-69100, Villeurbanne, France

²Department of Materials, ETH Zürich, 8093 Zürich, Switzerland.

³Yale University, New Haven, Connecticut 06520, USA.

⁴Institute of Science and Technology Austria (ISTA), Am Campus 1, 3400 Klosterneuburg, Austria.

⁵Department of Materials Science and Engineering,
Department of Physics, Cornell University, Ithaca, NY, USA.

(Dated: September 15, 2025)

Soft solids and their surface deformations control the response of many natural and artificial systems. Yet, their underlying properties are vigorously debated, particularly for polymer networks. While molecular-scale theories predict no interfacial changes with macroscopic deformation, multiple experiments suggest otherwise. To settle this issue, we measure displacement fields near the interface of a silicone gel, in the limit of small deformations. We discover an unexpected multiscale response. The shear modulus decreases smoothly by half with 20 μm of the interface. At the same time we observe a surface excess elasticity, that depends on history and outer medium composition. These results reveal the fundamentally multiscale nature of polymeric surfaces, and call for further experimental and theoretical investigations into the basic understanding of soft solid interfaces.

INTRODUCTION

Interfaces play a crucial role in mechanics and materials. They are central to composites and robotics [1–4], adhesion and friction [5–9], fracture [10–12], wetting [13–17], shape morphing [18–20], and mechanobiological processes in cells and tissues [21–23]. For solids, interfacial tension can play a dominant role at length scales smaller than the *elastocapillary length*, equal to the ratio of interfacial tension, Υ and shear modulus, μ [24–26]. This cross-over is widely accepted, but the fundamental nature of interfacial tension for soft polymeric solids is still controversial. In theory, ideal polymer chains should seamlessly rearrange at a deformed solid interface, leading to a strain-independent interfacial tension [27]. In practice, observations of microscopic deformations in silicone gels suggest a strain-dependent interfacial tension [15, 28–31]. The interpretation of these previous experiments, however, is complicated by material and geometric nonlinearities [32–35].

In this paper, we quantify mechanical properties near the interface of a silicone gel with high precision 3D location and tracking (Supplementary Section 1). We apply homogeneous or localized stresses, and analyze deformation fields in the linear response regime. First, we find a two-fold drop of the shear modulus, within 20 μm of the surface. Second, we find a surface excess elastic response, at unresolved scales, that depends on the composition of the surrounding medium and on deformation history. These results demonstrate the multiscale nature of soft polymeric solid interfaces, in contrast with the scale-free elastic models that are used widely to infer traction stresses or bulk elastic moduli [36–41]. We thus

need new approaches to understand, model, and design interfaces that account for their multiple intrinsic length scales.

EXPERIMENTAL DESIGN

We deform films of soft silicone gels in two geometries. First, we apply a simple shear stress (Fig. 1A) with a magnet adhered to the top of the film (Supplementary Section 2). This creates a homogeneous stress throughout the material. In this way, nonlinearities in strain pro-

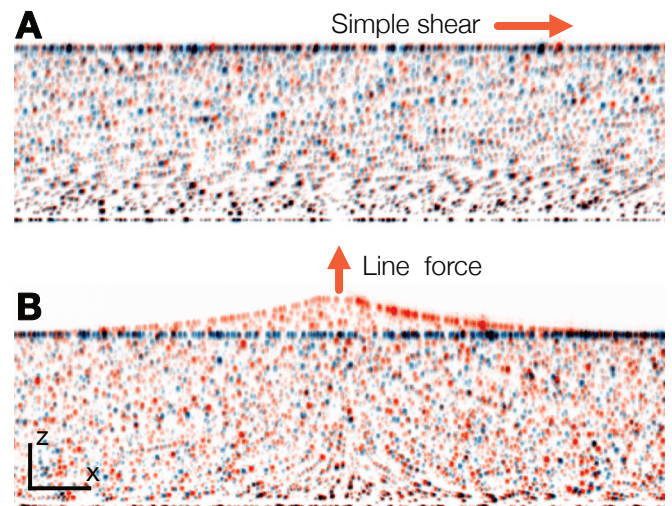


Fig. 1. Superimposed max-intensity projections of confocal stacks, before deformation (blue) and after deformation (orange), in two deformation modes (fraction of data - 10%). (A) Simple shear. (B) Line force. The scale bars defining the axis each equate 10 μm .

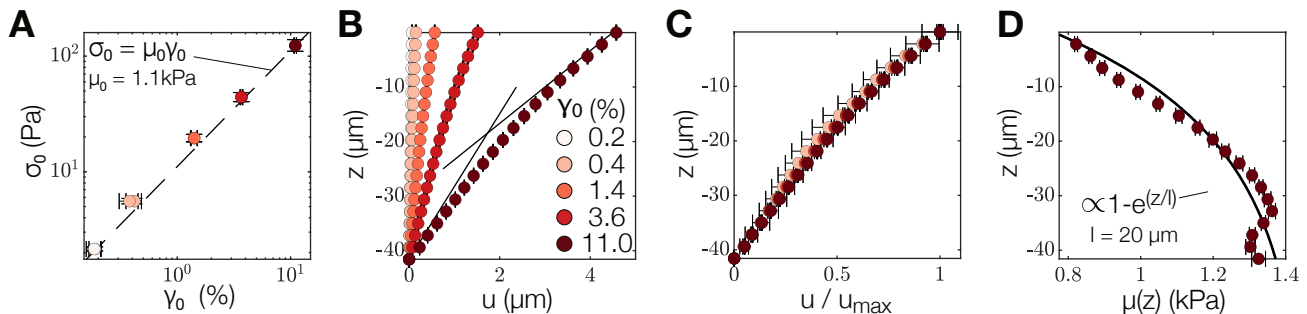


Fig. 2. (A) Bulk strain-stress relationship, together with the line $\sigma_0 = \mu_0 \gamma_0$ with $\mu_0 = 1.1 \text{ kPa}$. Errors bars correspond to twice the standard deviation. (B) Horizontal displacements u against the vertical position z . The black lines correspond to a linear fit of the first two and the last two dark red data points. (C) Horizontal displacements normalized by the maximal horizontal displacement u_{max} . (D) Local shear modulus $\mu(z)$ against the vertical position z . Each color codes for an imposed macroscopic stress. Plots (B)-(D) correspond to values averaged over $2.2 \mu\text{m}$ thick horizontal bins. The size of the errorbars equates twice the standard error of the mean (Supplementary Section 4).

files reveal material heterogeneities. Second, we apply a localized force per unit length, using the three-phase contact line of a liquid droplet (Fig. 1B) or from the edge of an adhered coverslip (Supplementary Section 3). In the latter experiments, observation of shear stresses at the interface reveals strain-dependent interfacial tension. In each case, we precisely measure the deformation fields with confocal microscopy of embedded quantum dots (Supplementary Video 1). The small size of these fluorescent tracers allows us to densely sample the deformation field, with an average spacing of $3 \mu\text{m}$, at vanishingly small volume fractions (10^{-5}). This allows us to quantify strains as small as 0.2% in x, y and 0.4% in z (Supplementary Section 1.4).

SIMPLE SHEAR REVEALS NEAR-SURFACE GRADIENTS IN BULK ELASTICITY

We measure three-dimensional deformation fields across the thin silicone film, as we increase the applied shear stress with a calibrated magnet-based setup (Fig. 1A, Supplementary Section 2). The average shear strain across the film is $\gamma_0 = [u(h) - u(0)]/h$, where u is the horizontal displacement and h the thickness of the sample. It increases linearly with the applied stress $\sigma_0 = \mu_0 \gamma_0$ (Fig. 2A), with a shear modulus of $\mu_0 = 1.1 \text{ kPa}$ consistent with previous experiments on this material [31].

We now investigate the local mechanical response through analysis of the full three-dimensional displacement field. As expected, we find that displacements only depend on z , and are independent of x and y (Supplementary Section 2.3). The z -dependence of the displacements are shown in Fig. 2B. Instead of the linear profile expected for a homogeneous material, we observe that the horizontal motion of the tracers decays non-linearly, faster close to the top surface (Fig. 2B, Supplementary Section 2.4). This behavior is independent of strain, over the range of measured values from 0.4% to 11.0%, as

shown by the collapse of displacement profiles on a single curve when normalized by the maximal displacement (Fig. 2C).

Since force balance requires the stress to be homogeneous, the non-linear displacement profile implies a heterogeneous shear modulus, $\mu(z) = \sigma_0 / \gamma(z)$, with $\gamma(z) = \partial u / \partial z$. The depth dependence of the shear modulus is shown in Fig. 2D. The shear modulus nearly doubles, from $765 \pm 3 \text{ Pa}$ at the top surface, to $1320 \pm 20 \text{ Pa}$ at the bottom surface. Its profile is in reasonable agreement with an exponential decay, with decay length $l = 20 \mu\text{m}$ (Fig. 2D). This gradient of shear modulus suggests a gradient in the network crosslinking density. Its profile is consistent with a reaction-diffusion process [42, 43], such as oxygen-inhibition of cross-linking [44]. The precise origin of this heterogeneity is however unknown and left for future investigation (Supplementary Section 2.5).

FORCE BALANCE AT INTERFACES

The net force on any part of a material at rest must equal zero. For volume elements spanning the interface, this force balance includes the bulk elastic stress $\boldsymbol{\sigma}$ and the interfacial excess stress Υ . When applied to the normal forces, we arrive at the familiar Laplace equation: $\mathbf{n} \cdot \boldsymbol{\sigma} \cdot \mathbf{n} = \sigma_{\text{nn}} = \kappa \Upsilon$, where κ is the local curvature, and \mathbf{n} the unit vector normal to the surface. When applied in-plane, the shear stress is balanced by the gradient of interfacial stress: $\mathbf{t} \cdot \boldsymbol{\sigma} \cdot \mathbf{n} = \sigma_{\text{tn}} = \partial \Upsilon / \partial s$, where \mathbf{t} is the unit vector tangent to the surface, and s is the arc-length material coordinate [24, 33]. In liquids, this is called the Marangoni stress [45]. Therefore, the shear stress must be non-zero when interfacial tension is heterogeneous. In the following, we extrapolate bulk stresses to the interface, and identify the interfacial tension gradient $\partial \Upsilon / \partial s$ as the tangential component of the unbalanced elastic stress.

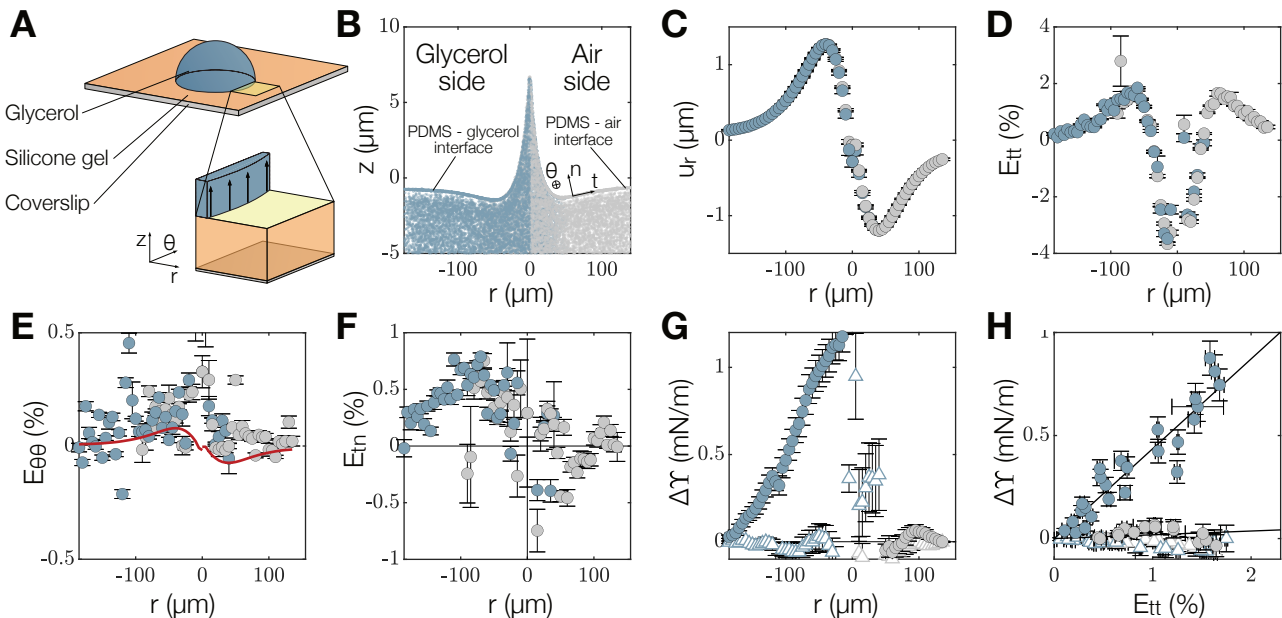


Fig. 3. (A) Sketch of the three-phase contact line confocal imaging. We acquire confocal stacks of both the inner and the outer side of the contact line. Sketches not to scale. (B) Azimuthally-collapsed quantum dots positions on both sides of the wetting ridge. Surface-deposited tracers are distinguishable from the bulk-included quantum dots. \mathbf{t} , \mathbf{n} , and $\boldsymbol{\theta}$ represent the unit vectors respectively tangent, normal to the surface, and in the orthoradial direction. (C) Surface radial displacement u_r . (D), (E), and (F) Surface tangential strain E_{tt} , orthoradial strain $E_{\theta\theta}$, and shear strain E_{tn} . In (F), the red curve corresponds to the expected orthoradial component u_r/R . (G) and (H) Excess interfacial tension $\Delta\Upsilon$ against the radial position r , and against the surface strain E_{tt} . In (H), the solid lines correspond to $\Delta\Upsilon = \Lambda E_{tt}$, with $\Lambda = 1.8$ mN/m, and $\Lambda = 43.6$ mN/m. In (C) to (H), the symbols correspond to values averaged over $5 \mu\text{m}$ wide radial bins, and the size of the errorbars equate twice the standard error of the mean (Supplementary Section 4). The filled circles correspond to measured values, and the non-filled triangles in (G) and (H) to bulk-extrapolated values. In (B) to (H), the blue and gray colors correspond to confocal datasets with most of the field of view on the glycerol and air sides, respectively.

STRESS GRADIENTS UNVEIL INTERFACE ELASTICITY

We measure three-dimensional deformation fields near the three phase contact line of a glycerol droplet resting on a thin silicone film (Figs. 1B, 3A, Supplementary Section 5.1). The interfacial tension of the liquid-air interface induces large deformations near the contact line [46]. Azimuthally-collapsed tracer positions near the contact line in are shown in Fig. 3B, and the radial displacement u_r of the surface in Fig. 3C (see Supplementary Section 5.2 for a 3D profile). Previous analyses of these profiles, which focused on the structure of the tip of the wetting ridge [46], were vulnerable to elastic singularities and solvent extraction [17, 32, 33, 47]. Here, we instead focus our analysis *far from the contact line*, where the deformations remain small.

To determine the bulk elastic stresses at the interface, we calculate the Green strain $\mathbf{E} = (\mathbf{F}^T \mathbf{F} - \mathbf{I})/2$, where $\mathbf{F} = \mathbf{I} + \nabla \mathbf{u}$ is the deformation gradient tensor, and assume Neo-Hookean behavior $\boldsymbol{\sigma} = 2\mu(z)\mathbf{E} - p\mathbf{I}$, where p is a pressure term [48]. We project the strain of the surface points onto the following coordinate system: we choose \mathbf{t} to be the unit vector tangent to the surface pointing in the radial direction, \mathbf{n} the unit vector normal to the

surface, and $\boldsymbol{\theta} = \mathbf{n} \times \mathbf{t}$ the unit vector in the orthoradial direction (Fig. 3B, Supplementary Section 5.3). The surface strain in the tangential direction, $E_{tt} = \mathbf{t} \cdot \mathbf{E} \cdot \mathbf{t}$, is shown in Fig. 3D. The profile is roughly symmetric about the contact line. Within $100 \mu\text{m}$ of the contact line, the strain is relatively large and quickly varying. Further away, it decays smoothly to zero. The strain in the orthoradial direction, $E_{\theta\theta} = \boldsymbol{\theta} \cdot \mathbf{E} \cdot \boldsymbol{\theta}$, is shown in Fig. 3E. It is much smaller than the strain in the radial direction. As all displacements only depend on r and z , the magnitude of $E_{\theta\theta}$ is comparable to u_r/R , shown in red, where u_r is the radial displacement and R the droplet radius [49]. Last, the shear strain $E_{tn} = \mathbf{t} \cdot \mathbf{E} \cdot \mathbf{n}$, shown in Fig. 3F, is asymmetric about the contact line.

Applying the Marangoni boundary condition, we calculate the incremental interfacial tension $\Delta\Upsilon = 2\mu(h) \int E_{tn} ds$ on either side of the contact line by integrating the shear strain from the far field along the arc-length s (Fig. 3G) [33]. At the PDMS-glycerol interface, the shear strain is positive (Fig. 3F). As a result, the incremental tension increases as the contact line is approached (Fig. 3G). When compared to the tangential strain E_{tt} , we find a linear increase in incremental tension (Fig. 3H). This suggests a linear elastic response of the interface: $\Delta\Upsilon = \Lambda E_{tt}$ with a surface modulus

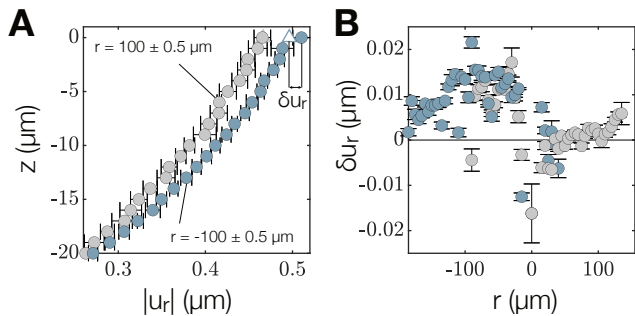


Fig. 4. Radial displacement surface jump. (A) Radial absolute displacement profile, at $-100 \mu\text{m} \pm 0.5 \mu\text{m}$ (blue) and $100 \mu\text{m} \pm 0.5 \mu\text{m}$ (gray) from the position of the wetting ridge, against vertical position z . Each symbol corresponds to values averaged over $1 \mu\text{m} \times 1 \mu\text{m}$ r - z bins. The circles correspond to measured displacements, and the triangle to bulk-extrapolated displacements. (B) Radial displacement jump against radial position r , same color-code as in Fig. 3. Each circle corresponds to surface values averaged over $5 \mu\text{m}$ wide radial bins. In (A) and (B), the size of the errorbars equate twice the standard error of the mean (Supplementary Section 4).

$\Lambda = 43.6 \pm 4.5 \text{ mN/m}$. In contrast, the shear strain on the PDMS-air side fluctuates about zero (Fig. 3F). The incremental tension therefore does not significantly deviate from zero (Fig. 3G), and when compared to the surface strain, it gives $\Lambda = 1.8 \pm 1.7 \text{ mN/m}$. Thus, the interfacial tension of the PDMS-air interface is effectively independent of surface strain. The contrast in interface elasticity across the contact line was observed consistently across five different instances (Supplementary Section 5.4), and complemented with additional measurements on the deformed PDMS-air interface at the edge of the coverslip (Supplementary Section 6).

DISPLACEMENT JUMP REVEALS SURFACE ALTERATION

To isolate the features of the data that encode surface elasticity, we examine the radial displacement vertical profile $u_r(z)$ (Fig. 4A). On the air side, where no surface elasticity is observed, $u_r(z)$ increases smoothly from bottom to top. On the glycerol side, where we observed significant surface elasticity, $u_r(z)$ jumps when reaching the top surface. This discontinuity occurs over a sub-micron length scale, much smaller than the elasticity gradient described above, and differs from previously reported interface slippage in which bulk and surface move as one [50, 51]. We quantify the jump amplitude, δu_r , as the difference between measured and bulk-extrapolated surface displacements (Fig. 4B). We find it to be of the order of 10 nm along the PDMS-glycerol interface, and close to 0 nm along the PDMS-air interface.

We test the significance of the displacement jump by reanalyzing the data excluding tracers attached to the

surface (Supplementary Section 7). In this case, interfacial tension appears to be independent of surface strain on both sides of the interface (Fig. 3G and H). In other words, the observed displacement jump at the top surface is responsible for the measured interfacial elasticity. We report this systematic behavior in the other samples we tested in Supplementary Section 8.

Among the phenomena that might lead to observed differences in the surface response on the two sides of the interface, we verified that the shear stress on the glycerol side could neither be explained by an optical artifact (Supplementary Section 9), nor by hydrodynamic flows (Supplementary Video 2). We are thus left with two hypotheses. First, molecular interactions between glycerol and PDMS. On one hand, we estimated that glycerol swells this silicone gel by less than 3ppm (Supplementary Section 10), making localized changes to material properties due to the dissolution of glycerol into polymer network unlikely [52, 53]. On the other hand, recent experiments have shown that oxygen along the backbone of PDMS anchors to glycerol [54], which could lead to conformational changes of silicone molecules over a molecularly thin layer. Second, mechanical damage. As the glycerol droplet is grown to its final shape, the PDMS undergoes large deformation at the wetting ridge and permanent damage could alter the mechanical behavior over a thin layer [55]. This hypothesis would be consistent with recent surface elasticity measurements on a soft PDMS after it was peeled off from a patterned mold [31].

Whether the surface apparent surface elasticity has a chemical or a mechanical origin calls for further investigations. These results however demonstrate that surface elasticity can be tuned independently of bulk properties by the mere passage of a liquid drop, highlighting the fundamental nature of interface elasticity as an interfacial property and opening the way for its direct engineering.

DISCUSSION AND CONCLUSION

We measured bulk and interface properties of a polymer gel through high-precision tracking of nanotracers under controlled deformations. We resolved a gradient of the shear modulus within $20 \mu\text{m}$ of the interface, and quantified an environment-dependent interface excess elasticity that arises from a mechanical discontinuity over an unresolved length scale.

These results suggest a hierarchy of length scales associated with the interface, and invite us to think carefully about the definition of interfacial properties. Interfacial properties, as defined by Gibbs, emerge from the variation of some bulk property over an unresolved length scale near an interface [56]. This definition does *not* assume that interfacial excess properties emerge at the smallest structural scale, just that they are unresolved. Interfacial properties can therefore arise from

excess quantities spanning over molecular or supramolecular scales. In a polymer network, interfacial properties could be defined at the monomer scale, the mesh scale, or over larger length scales defined by network heterogeneities.

In our experiments, depth-dependent moduli, varying over tens of microns, suggest network heterogeneities. By contrast, interface elasticity emerges at an unresolved (*i.e.* sub-micron) scale. It is incompatible with the molecular view of ideal polymer networks, whose flexible chains make interfacial properties independent of deformation [27]. Since interface elasticity is observed against glycerol, but not against air, we suspect either that mesh-bound moieties are anchored to the interface in glycerol but not in air, or that large deformation at the wetting ridge resulted in surface-localized damage. Indeed, recent experiments [54] have shown that oxygen along the backbone of PDMS is anchored to glycerol and can prevent fusion of glycerol droplets in silicone oil, and others have shown that a PDMS surface which was peeled off a mold exhibits a net interfacial elasticity [31].

These observations demand a fresh perspective on the interfacial properties and mechanical response of soft polymer solids. From a polymer science perspective, we need a clear understanding of the molecular and mesh-scale features that can govern interface elasticity and better control of crosslinking to avoid or enhance larger scale network heterogeneities. From a mechanical perspective, we need clear framework for modeling materials with a multi-scale interfacial response. While most experiments characterizing polymer networks at the micron-scale assume a scale-free response (*e.g.* Hertzian contact mechanics [57] or traction force microscopy [37, 58]), our results show that there are at least four length scales in the problem: the elastocapillary length (Υ/μ), a length scale associated with interface elasticity (Λ/μ), the length scale of network heterogeneity (l), and the length scale of displacement discontinuity. In the current experiments, the three former length scales are roughly $20\ \mu\text{m}$, and the latter is unresolved (*i.e.* sub-micron). We expect these values to differ in other systems. The resulting mechanical response would then qualitatively differ, depending on the relative values of all length scales at play.

AUTHOR CONTRIBUTIONS:

N.B. and E.R.D. conceived the project and designed the experiments. L.A.W. designed and made the magnetic holder, and performed the magnet calibration curves. S.D., K.V., and H.K. performed the swelling and the NMR measurements. D.G. performed the glycerol flooding measurement. N.B. performed all the other experiments. N.B. analyzed all the experiments. N.B. and E.R.D. interpreted the experiments, with input from M.Z., C.P.G., and R.W.S. N.B. and E.R.D. wrote the pa-

per with inputs from all authors. E.R.D. and N.B. supervised the project.

ACKNOWLEDGEMENTS:

The authors thank Katharine Jensen, Stefanie Heyden, Thomas Salez, Francesco Stellacci, Denis Bartolo, Francesco Picella, H el ene Delano -Ayari, Mathieu Leocmach, Antoine B erut, C ecile Cottin-Bizonne, Anne-Laure Bianco, and Oriane Talabart for useful discussions.

* nicolas.bain@cnr.fr

- [1] R. H. Baughman, A. A. Zakhidov, and W. A. De Heer, *science* **297**, 787 (2002).
- [2] R. W. Style, R. Boltyanskiy, B. Allen, K. E. Jensen, H. P. Foote, J. S. Wettlaufer, and E. R. Dufresne, *Nature Physics* **11**, 82 (2015).
- [3] V. M. Ortega-Jimenez, D. Kim, S. Kumar, C. Kim, J.-S. Koh, and S. Bhamla, *Science* **389**, 811 (2025).
- [4] J.-S. Koh, E. Yang, G.-P. Jung, S.-P. Jung, J. H. Son, S.-I. Lee, P. G. Jablonski, R. J. Wood, H.-Y. Kim, and K.-J. Cho, *Science* **349**, 517 (2015).
- [5] S. Karpitschka, L. van Wijngaarden, and J. H. Snoeijer, *Soft Matter* **12**, 4463 (2016).
- [6] C.-Y. Hui, Z. Liu, N. Bain, A. Jagota, E. R. Dufresne, R. W. Style, R. Kiyama, and J. P. Gong, *Proceedings of the Royal Society A* **476**, 20200477 (2020).
- [7] B. Saintyves, T. Jules, T. Salez, and L. Mahadevan, *Proceedings of the National Academy of Sciences* **113**, 5847 (2016).
- [8] S. Lee and N. D. Spencer, *Science* **319**, 575 (2008).
- [9] C. Creton, *MRS bulletin* **28**, 434 (2003).
- [10] J. B. Bostwick and K. E. Daniels, *Physical Review E—Statistical, Nonlinear, and Soft Matter Physics* **88**, 042410 (2013).
- [11] Q. Liu, T. Ouchi, L. Jin, R. Hayward, and Z. Suo, *Physical review letters* **122**, 098003 (2019).
- [12] C. Creton and M. Ciccotti, *Reports on Progress in Physics* **79**, 046601 (2016).
- [13] P.-G. De Gennes, *Reviews of modern physics* **57**, 827 (1985).
- [14] C. Duprat, S. Protiere, A. Beebe, and H. A. Stone, *Nature* **482**, 510 (2012).
- [15] A. Bardall, K. E. Daniels, and M. Shearer, *European Journal of Applied Mathematics* **29**, 281 (2018).
- [16] E. R. Jerison, Y. Xu, L. A. Wilen, and E. R. Dufresne, *Physical review letters* **106**, 186103 (2011).
- [17] Z. Cai, A. Skabeev, S. Morozova, and J. T. Pham, *Communications Materials* **2**, 21 (2021).
- [18] J. Bico,  . Reyssat, and B. Roman, *Annual Review of Fluid Mechanics* **50**, 629 (2018).
- [19] D. Paretkar, X. Xu, C.-Y. Hui, and A. Jagota, *Soft matter* **10**, 4084 (2014).
- [20] S. Mora, C. Maurini, T. Phou, J.-M. Fromental, B. Audoly, and Y. Pomeau, *Physical review letters* **111**, 114301 (2013).
- [21] S. Ehrig, B. Schamberger, C. M. Bidan, A. West, C. Jacobi, K. Lam, P. Kollmannsberger, A. Petersen,

- P. Tomancak, K. Kommareddy, *et al.*, *Science advances* **5**, eaav9394 (2019).
- [22] X. Shi, Z. Liu, L. Feng, T. Zhao, C.-Y. Hui, and S. Zhang, *Physical Review X* **12**, 021053 (2022).
- [23] M. S. Yousafzai, V. Yadav, S. Amiri, M. F. Staddon, Y. Errami, G. Jaspard, S. Banerjee, and M. Murrell, *Physical Review X* **12**, 031027 (2022).
- [24] R. W. Style, A. Jagota, C.-Y. Hui, and E. R. Dufresne, *Annual Review of Condensed Matter Physics* **8**, 99 (2017).
- [25] B. Andreotti and J. H. Snoeijer, *Annual review of fluid mechanics* **52**, 285 (2020).
- [26] L. Chen, E. Bonaccorso, T. Gambaryan-Roisman, V. Starov, N. Koursari, and Y. Zhao, *Current opinion in colloid & interface science* **36**, 46 (2018).
- [27] H. Liang, Z. Cao, Z. Wang, and A. V. Dobrynin, *ACS Macro Letters* **7**, 116 (2018).
- [28] Q. Xu, K. E. Jensen, R. Boltynskiy, R. Sarfati, R. W. Style, and E. R. Dufresne, *Nature communications* **8**, 1 (2017).
- [29] K. E. Jensen, R. W. Style, Q. Xu, and E. R. Dufresne, *Physical Review X* **7**, 041031 (2017).
- [30] Q. Xu, R. W. Style, and E. R. Dufresne, *Soft Matter* **14**, 916 (2018).
- [31] N. Bain, A. Jagota, K. Smith-Mannschott, S. Heyden, R. W. Style, and E. R. Dufresne, *Physical Review Letters* **127**, 208001 (2021).
- [32] R. Masurel, M. Roché, L. Limat, I. Ionescu, and J. Derieux, *Physical review letters* **122**, 248004 (2019).
- [33] A. Pandey, B. Andreotti, S. Karpitschka, G. Van Zwieten, E. Van Brummelen, and J. Snoeijer, *Physical Review X* **10**, 031067 (2020).
- [34] S. Heyden, P. M. Vlahovska, and E. R. Dufresne, *Journal of the Mechanics and Physics of Solids* **161**, 104786 (2022).
- [35] S. Heyden and N. Bain, *Soft Matter* **20**, 5592 (2024).
- [36] M. Radmacher, R. Tillmann, M. Fritz, and H. Gaub, *Science* **257**, 1900 (1992).
- [37] R. W. Style, R. Boltynskiy, G. K. German, C. Hyland, C. W. MacMinn, A. F. Mertz, L. A. Wilen, Y. Xu, and E. R. Dufresne, *Soft matter* **10**, 4047 (2014).
- [38] B. C. Cheung, R. J. Abbed, M. Wu, and S. E. Leggett, *Annual Review of Biomedical Engineering* **26** (2024).
- [39] M. D. Norman, S. A. Ferreira, G. M. Jowett, L. Bozec, and E. Gentleman, *Nature Protocols* **16**, 2418 (2021).
- [40] J.-P. Rieu, C. Barentin, Y. Maeda, and Y. Sawada, *Biophysical journal* **89**, 3563 (2005).
- [41] H. Delanoë-Ayari, J. Rieu, and M. Sano, *Physical Review Letters* **105**, 248103 (2010).
- [42] A. M. Turing, *Bulletin of mathematical biology* **52**, 153 (1990).
- [43] S. Kondo and T. Miura, *science* **329**, 1616 (2010).
- [44] J. Mandal, K. Zhang, N. D. Spencer, *et al.*, *Soft Matter* **17**, 6394 (2021).
- [45] L. Scriven and C. Sternling, *Nature* **187**, 186 (1960).
- [46] R. W. Style, R. Boltynskiy, Y. Che, J. Wettlaufer, L. A. Wilen, and E. R. Dufresne, *Physical review letters* **110**, 066103 (2013).
- [47] M. M. Flapper, A. Pandey, M. Essink, E. Van Brummelen, S. Karpitschka, and J. Snoeijer, *Physical review letters* **130**, 228201 (2023).
- [48] C. W. Barney, C. Chen, and A. J. Crosby, *Soft Matter* **17**, 5574 (2021).
- [49] L. D. Landau and E. M. Lifshitz, *Mechanics*, Vol. 1 (CUP Archive, 1960).
- [50] B.-m. Z. Newby, M. K. Chaudhury, and H. R. Brown, *Science* **269**, 1407 (1995).
- [51] B.-m. Zhang Newby and M. K. Chaudhury, *Langmuir* **13**, 1805 (1997).
- [52] J. N. Lee, C. Park, and G. M. Whitesides, *Analytical chemistry* **75**, 6544 (2003).
- [53] S.-Y. Chen, A. Bardall, M. Shearer, and K. E. Daniels, *Soft Matter* **15**, 9426 (2019).
- [54] C. Nannette, J. Baudry, A. Chen, Y. Song, A. Shglabow, N. Bremond, D. Démoulin, J. Walters, D. A. Weitz, and J. Bibette, *Science* **384**, 209 (2024).
- [55] S. K. Thanawala and M. K. Chaudhury, *Langmuir* **16**, 1256 (2000).
- [56] J. W. Gibbs, *American Journal of Science* **3**, 441 (1878).
- [57] K. L. Johnson, *Contact mechanics* (Cambridge university press, 1987).
- [58] A. K. Harris, P. Wild, and D. Stopak, *Science* **208**, 177 (1980).
- [59] S. Deguchi, J. Hotta, S. Yokoyama, and T. S. Matsui, *Journal of Micromechanics and Microengineering* **25**, 097002 (2015).
- [60] J. Y. Kim, S. Heyden, D. Gerber, N. Bain, E. R. Dufresne, and R. W. Style, *Phys. Rev. X* **11**, 031004 (2021).
- [61] A. Iske, *Multiresolution methods in scattered data modelling*, Vol. 37 (Springer Science & Business Media, 2004).
- [62] J. Jonkman, C. M. Brown, G. D. Wright, K. I. Anderson, and A. J. North, *Nature protocols* **15**, 1585 (2020).
- [63] A. Testa, M. Dindo, A. A. Rebane, B. Nasouri, R. W. Style, R. Golestanian, E. R. Dufresne, and P. Laurino, *Nature communications* **12**, 6293 (2021).